Precision Control and Compensation of Servomotors and Machine Tools via the Disturbance Observer

Wei-Sheng Huang, Chun-Wei Liu, Pau-Lo Hsu, *Member, IEEE*, and Syh-Shiuh Yeh

***Abstract*—The computerized numerical control machine tool is a highly integrated mechatronic system in manufacturing processes. However, uncertainties degrade its motion accuracy. These include modeling errors, parameter variation, friction, and measurement errors that are present in either linear or nonlinear nature. In this paper, a state-space disturbance observer was successfully applied to servomotors to estimate and compensate for the uncertainties of parameter variation and current measurement problems, in the velocity and current loops, respectively. Furthermore, an autotuning procedure was developed accordingly to identify the varied parameters of the motor. Furthermore, by implementing the present servomotor systems in high-precision machine tools, the nonlinear friction compensation was adopted to reduce the slip-stick effect in contouring motion. Experimental results indicate that the roundness error has been significantly reduced from 13.3 to 2.0 μm by applying the proposed approaches.**

***Index Terms*—Contouring, disturbance, friction, identification, inertia, machine tool control, motion tool, observer, servomotor, viscous.**

NOMENCLATURE

T_e	Electromechanical torque.
T_L	External force and disturbance torque.
i_q	Electromechanical torque current.
K_t	Torque constant of the motor.
J	Equivalent motor and load inertia.
B	Friction viscous coefficient.
ω	Motor velocity.
$\overline{J}$	Normalized inertia.
$\overline{B}$	Viscous coefficient.
$\widetilde{d}$	Digital disturbance observer (DOB) estimated output.
n	Measurement noise.
T_e	Motor torque.
i_L	External disturbance.
i_F	Sum of static, Coulomb, and viscous friction.

Manuscript received January 5, 2009; revised September 30, 2009. First published October 23, 2009; current version published December 11, 2009. This work was supported in part by the National Science Foundation under Contract NSC 96-2218-E-009-021, in part by Mirle Company, and in part by Syntec Company.

W.-S. Huang, C.-W. Liu, and P.-L. Hsu are with the Department of Electrical and Control Engineering, National Chiao Tung University, Hsinchu 300, Taiwan (e-mail: plhsu@cc.nctu.edu.tw).

S.-S. Yeh is with the Department of Mechanical Engineering, National Taipei University of Technology, Taipei 10608, Taiwan.

Color versions of one or more of the figures in this paper are available online at http://ieeexplore.ieee.org.

Digital Object Identifier 10.1109/TIE.2009.2034178

I. INTRODUCTION

SERVOMOTORS implemented in computerized numerical control (CNC) machine tools are widely applied to modern manufacturing processes to ensure precision of machining products. Unavoidably, uncertainties may seriously degrade motion precision occurring in the current loop, velocity, and position loops. In general, the current measurement error exists in the motor driver because of the noise, and calibration is thus required; however, friction in the machine table becomes more serious, owing to the aging problem. Moreover, the load and external cutting force are varied in practice. All those uncertainties are mutually coupled in different loops and lead to the degradation of motion accuracy in real applications using precise model design.

Recently, advanced control strategies have been developed for servomotors and CNC machine tools. In the current loop of the servomotor, space vector pulsewidth modulation [1], [2] has been widely adopted to achieve less switching on power electronics with reduced harmonic components. Given that the current loop provides the desirable torque for the motor and the machine, the measurement errors on the current loop and the cogging torque of the motor will inevitably cause torque ripple and oscillation during motion. Basically, most advanced motion control theories focus on either the velocity loop or the position loop [3]–[6]. To achieve motion precision for the CNC machine tool, the position, velocity, and current loops must be designed to effectively reduce those uncertainty effects to achieve improved precision. The proportional–integral–derivative (PID) control is still widely used in all three loops because of its reliability and ease of adjustment. In fact, the performance of the PI-controlled CNC servo system, usually with a higher bandwidth and less overshoot, is very sensitive to most uncertainties. Therefore, more effective approaches to achieve higher motion precision against uncertainties are still pursued in manufacturing processes.

In real applications, if the sources of disturbance and uncertainties can be properly identified, appropriate actions can be taken accordingly with further compensation. The DOB is efficient for disturbance estimation and rejection [7]. Kobayshi *et al.* [8] developed the phase compensation based on the disturbance observer to cope with parameter variation in motor systems. Meanwhile, Katsura *et al.* [9] adopted the accelerometer to achieve a torque observer with a wide bandwidth, while Lee and Blaabjerg [10] applied the inertia observer to estimate the inertia at low-speed performance. She *et al.* [11] proposed the estimation of an equivalent input disturbance to improve disturbance rejection for servomotor control systems.

To suppress all uncertainty effects on both current and velocity loops of servomotors, this paper adopts the state-space DOB modeling simply with the equivalent inertia and viscous coefficient. As a result, not only the DOB may suppress parameter variation with compensation in practice but its output will also indicate the quantity of variation for further monitoring. Moreover, the torque ripple observed in the velocity loop will also be effectively suppressed.

Basically, the DOB in different formats is a model-based design, and its output indicates the difference between the real plant and the nominal model [12]–[15]. When the plant is varied to some extents, an adaptive parameter estimation to update the model is proposed [16]. In addition to its applications to the CNC machine tool with a high-order transfer function model [17], the present DOB is a state-space modeling approach considering the velocity loop directly. Once the major physical parameter of inertia or viscous changes, the present DOB can be applied to properly acquire those real parameters.

Thus, by implementing the developed DOB-based servomotor control systems in a CNC machine tool, the nonlinear slip-stick phenomenon caused by friction can be properly estimated and eliminated by applying the nonlinear friction compensation (NFC) simply with a feedforward structure [18]. The proposed algorithm has been implemented on the TI DSP 2812 microcontroller for the Tamagawa ac 400-W servomotors. Furthermore, by implementing servomotors in a DYNA DM1007 CNC machine tool, friction in the tool table has been identified, and the NFC has been applied to the machine tool to effectively reduce the slip-stick effect on the contouring precision.

II. DOB-Based Suppression of Uncertainty

The state-space representation of a general dynamic plant can be expressed as

$$\begin{aligned}\mathbf{x}(k+1) &= \mathbf{\Phi}\mathbf{x}(k) + \mathbf{\Gamma}u(k)\\ y(k) &= \mathbf{H}\mathbf{x}(k).\end{aligned} \tag{1}$$

The DOB has been proposed to estimate and properly reduce the effect of external disturbance on the system [7]. In general, the disturbance d can be modeled in the state-space equation as

$$\begin{aligned}\mathbf{x}_d(k+1) &= \mathbf{\Phi}_d\mathbf{x}_d(k)\\ d(k) &= \mathbf{H}_d\mathbf{x}_d(k).\end{aligned} \tag{2}$$

Thus, the disturbance model can be further augmented with the system model as

$$\begin{aligned}\begin{bmatrix}\mathbf{x}(k+1)\\ \mathbf{x}_d(k+1)\end{bmatrix} &= \begin{bmatrix}\mathbf{\Phi} & \mathbf{\Gamma}\mathbf{H}_d\\ 0 & \mathbf{\Phi}_d\end{bmatrix}\begin{bmatrix}\mathbf{x}(k)\\ \mathbf{x}_d(k)\end{bmatrix} + \begin{bmatrix}\mathbf{\Gamma}\\ 0\end{bmatrix}u(k)\\ y &= [\mathbf{H} \quad 0]\begin{bmatrix}\mathbf{x}(k)\\ \mathbf{x}_d(k)\end{bmatrix}.\end{aligned} \tag{3}$$

Hence, the DOB is expressed as

$$\begin{aligned}\begin{bmatrix}\hat{\mathbf{x}}(k+1)\\ \hat{\mathbf{x}}_d(k+1)\end{bmatrix} &= \mathbf{\Phi}_\omega\begin{bmatrix}\hat{\mathbf{x}}(k)\\ \hat{\mathbf{x}}_d(k)\end{bmatrix}\\ &\quad + \mathbf{\Gamma}_\omega u(k) + \mathbf{L}\left(y - \mathbf{H}_\omega\begin{bmatrix}\hat{\mathbf{x}}(k)\\ \hat{\mathbf{x}}_d(k)\end{bmatrix}\right)\end{aligned} \tag{4}$$

with the gain matrix $\mathbf{L}$ designated to determine observer poles.

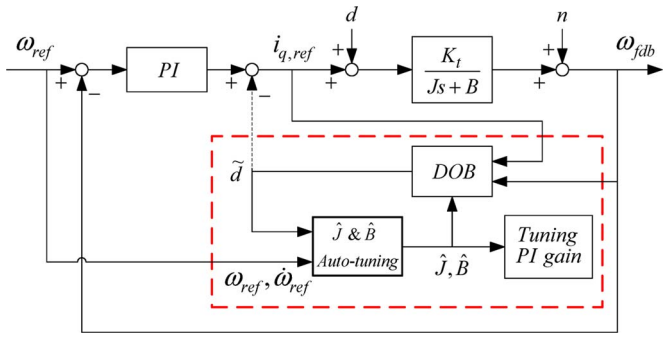

Fig. 1. DOB implementation for the servomotor with autotuning.

A. DOB Modeling for Servomotors

The velocity loop of the motor control is the modeling target for practical implementation of the DOB. Ideally, the motor current i_q generates the torque T_e to drive the mechanical equation as

$$\begin{aligned}T_e &= K_t \cdot i_q\\ T_e + T_L &= J\frac{d\omega}{dt} + B\omega\end{aligned} \tag{5}$$

where

T_e electromechanical torque;
T_L external force and disturbance torque;
i_q electromechanical torque current;
K_t torque constant of the motor;
J equivalent motor and load inertia;
B friction viscous coefficient;
ω motor velocity.

The DOB modeling and its extensive application of the autotuning process for the servomotor are shown in Fig. 1, where n is the measurement noise and $\tilde{d}$ is the DOB-estimated output that is directly fed to the current command to compensate for the lumped uncertain effects.

By considering the undesirable external disturbance, (5) of the servomotor is further normalized to K_t as

$$\overline{J}\frac{d\omega}{dt} + \overline{B}\omega = i_q + i_L \tag{6}$$

where the normalized inertia $\overline{J}$ and viscous coefficient $\overline{B}$ are the parameters in the DOB modeling. By applying the Euler's rule with the sampling time T_s, the discrete (6) becomes

$$\frac{\overline{J}}{T_s}(\omega(k+1) - \omega(k)) + \overline{B}\omega(k) = i_q(k) + i_L(k). \tag{7}$$

Therefore, by defining the system states of the DOB as the rotation velocity $\omega(k)$ and the external loading disturbance current $i_L(k)$ as

$$\begin{aligned}\begin{bmatrix}\hat{\omega}(k+1)\\ \hat{i}_L(k+1)\end{bmatrix} &= \mathbf{A}\begin{bmatrix}\hat{\omega}(k)\\ \hat{i}_L(k)\end{bmatrix}\\ &\quad + \mathbf{B}i_q^*(k) + \mathbf{L}\left(\omega(k) - \mathbf{C}\begin{bmatrix}\hat{\omega}(k)\\ \hat{i}_L(k)\end{bmatrix}\right)\end{aligned} \tag{8}$$

where

$$\mathbf{A} = \begin{bmatrix} 1 - \frac{\overline{B}T_s}{\overline{J}} & \frac{T_s}{\overline{J}} \\ 0 & 1 \end{bmatrix} \qquad \mathbf{B} = \begin{bmatrix} \frac{T_s}{\overline{J}} \\ 0 \end{bmatrix}$$

$$\mathbf{C} = [1 \quad 0] \qquad \mathbf{L} = \begin{bmatrix} l_1 \\ l_2 \end{bmatrix}$$

the DOB formulation can be implemented directly on the DSP microcontrollers by simply using the $\overline{B}$ and $\overline{J}$ parameters.

B. Variation of Parameters

Since uncertainties are unavoidable in real applications, the present DOB-based design, which lumps all undesirable disturbance, parameter variations, and modeling error, becomes a practical approach to suppress those uncertainties. In practice, parameter variation occurs as the operation changes, and the viscous coefficient increases as the duration increases. In addition, the bias and mismatched gains among the three-phase current sensors in the current loop of motor drivers generate the torque ripple effects. The output of the present DOB implementation indicates the deviation between the nominal model and the real system. If the output of DOB is small, as shown in Fig. 1, it implies that the parameters of the present modeling are accurate to some extent. Once the uncertainties of either external disturbance or internal parameter variation occur, the output of the DOB $\hat{d}$ will increase, and the estimated lumped disturbance $\hat{d}$ will be fed directly to its input to compensate for the effect of the uncertainties.

1) Viscous Coefficient: As the motor operation is at a constant speed without external disturbance, (6) simply becomes

$$\overline{B}\omega(k) = i_q(k). \tag{9}$$

If the estimated viscous coefficient $\overline{B}$ is greater than its actual value, (6) can be expressed as

$$\begin{aligned} \hat{B}\omega(k) &= (\overline{B} + \Delta B)\omega(k) \\ &= i_q(k) + i_L(k) \end{aligned} \tag{10}$$

where $\hat{B}$ is the estimated viscous, and ΔB is the difference between the estimated and actual values. Comparing (10) with (9), the DOB output i_L under a constant speed ω becomes the following value presented in the DOB output as:

$$i_L(k) = \Delta B\omega. \tag{11}$$

2) Inertia: If $\overline{B}$ has been accurately estimated and if the motor is operating at a constant acceleration or deceleration, (6) becomes

$$\frac{\overline{J}}{T_s}\left(\omega(k+1) - \omega(k)\right) + \overline{B}\omega(k) = i_q(k). \tag{12}$$

(a)

(b)

Fig. 2. Developed servomotor controller and the Tamagawa 400-W motor.

When the estimated inertia $\overline{J}$ is greater than its actual value, (6) further becomes

$$\begin{aligned} &\frac{\hat{J}}{T_s}\left(\omega(k+1) - \omega(k)\right) + \hat{B}\omega(k) \\ &\quad = \frac{\overline{J} + \Delta J}{T_s}\left(\omega(k+1) - \omega(k)\right) + \overline{B}\omega(k) \\ &\quad = i_q(k) + i_L(k) \end{aligned} \tag{13}$$

where ΔJ is the difference between the estimated $\hat{J}$ and the actual inertia J. Comparing (13) with (12), the DOB output then becomes

$$i_L(k) = \frac{\Delta J}{T_s}\left(\omega(k+1) - \omega(k)\right). \tag{14}$$

Thus, the DOB output is proportional to the model parameter error either at a constant speed or a constant acceleration/deceleration motion command.

C. Experimental Setup

To implement the designed DOB algorithm, experiments on the Tamagawa 400-W servomotor are shown in Fig. 2. The three-phase current was measured from the Hall sensor, and the velocity was measured from the 17-bit encoder with a

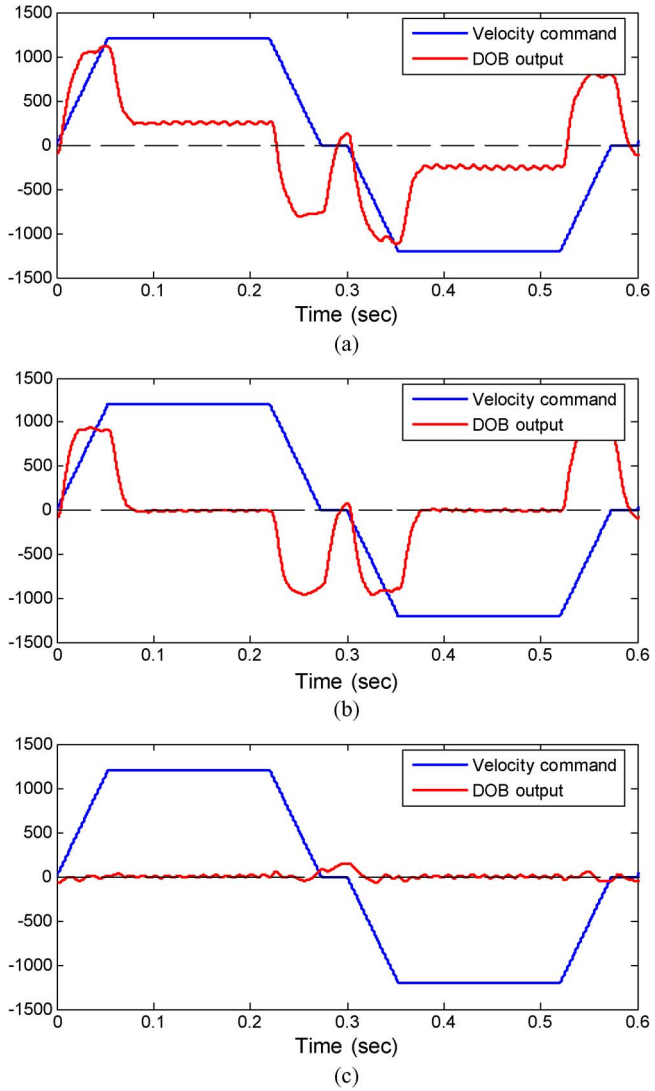

Fig. 3. Experiments of DOB output for estimation. (a) $\hat{B} > B$ and $\hat{J} > J$. (b) $\hat{B} = B$ and $\hat{J} > J$. (c) $\hat{B} = B$ and $\hat{J} = J$.

difference operator. All algorithms were implemented on the TI DSP 2812 microcontroller for both the servomotors and CNC machine tools.

D. Parameter Identification With Autotuning

The model-based DOB design not only can be applied to suppress model uncertainties but also can be adopted to achieve disturbance estimation and rejection. As discussed in (11) and (14), the effect of the viscous coefficient will mainly present as the motor operates at a constant speed, while the effect of the inertia will mainly present at a constant acceleration or deceleration in the DOB output. Thus, both parameters should be identified separately with different operation commands. The experimental results of the DOB output with erroneous B and J are shown in Fig. 3(a). The results shown in Fig. 3(b) indicate that the output of DOB is subject for elimination at a constant speed if a proper value of the viscous coefficient is provided. Furthermore, the output of DOB during acceleration/deceleration will also approach zero if the proper inertia is

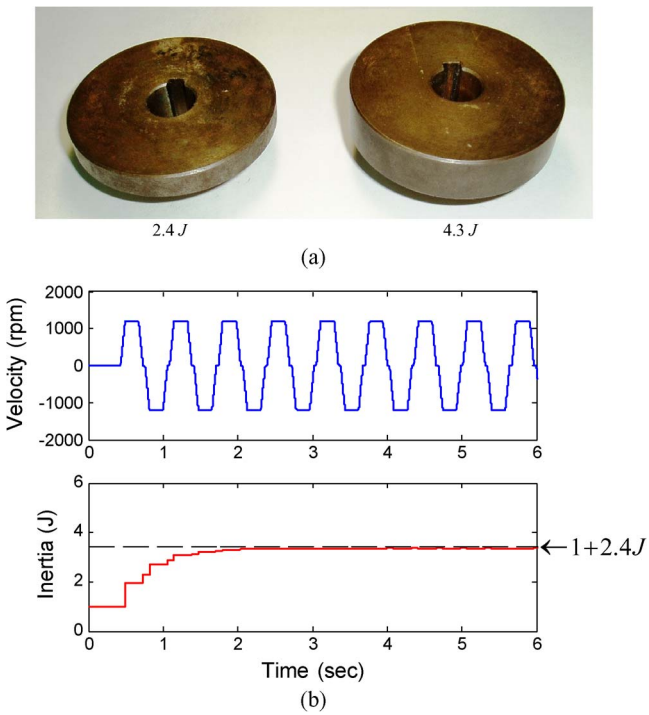

Fig. 4. (a) Additional inertia. (b) Autotuning results with an extra 2.4 J.

obtained, as shown in Fig. 3(c). These experimental results are in good agreement with analytical results in (11) and (14).

To further implement the aforementioned results in an automatic procedure, the simple integral autotuning process based on the estimated disturbance of DOB output, the estimated viscous coefficient $\hat{B}$, and the estimated inertia $\hat{J}$ can be achieved simply as in the following integral adaptive algorithm with suitable constants K_1 and K_2 as:

$$\begin{cases} \hat{B}(k+1) = \hat{B}(k) - K_1\tilde{d}(k+1) \\ \hat{J}(k+1) = \hat{J}(k) - K_2\tilde{d}(k+1). \end{cases} \tag{15}$$

Real-time tuning results are shown in Fig. 4. Additional 2.4 and 4.3 times the inertia of the motor rotor were tested, as shown in Fig. 4(a). After 6 s with nine-cycle learning, the algorithm applying (15) rendered a satisfactory result for both cases, as shown in Fig. 4(b). The results in Fig. 5(a) also show that the response becomes sluggish as the additional load is added. By applying the present autotuning process, a well-designed control performance can be restored, as shown in Fig. 5(b)

III. Suppression of Torque Ripple

A. Motor Current Measurement Error

For the control of permanent-magnet synchronized ac servomotors, only two of three stator currents are required to be measured with the Hall current sensor, while the third-phase current is directly calculated with the assumption of current balance. The three-phase motor model $(i_a - i_b - i_c)$ can be transformed into a synchronization coordinate $(i_d - i_q)$ by applying the Clark and Park transform as

$$\begin{cases} i_\alpha = i_a \\ i_\beta = (2i_b + i_a)/\sqrt{3} \end{cases} \tag{16}$$

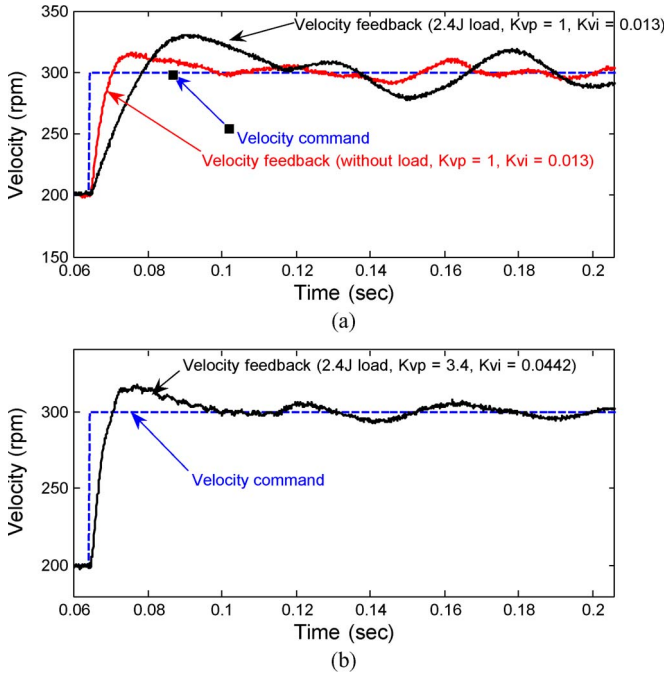

Fig. 5. (a) Responses as the 2.4-J inertia is added. (b) Restored performance after the autotuning procedure.

where

$$\begin{cases} i_d = i_\alpha \cos\theta + i_\beta \sin\theta \\ i_q = -i_\alpha \sin\theta + i_\beta \cos\theta. \end{cases} \tag{17}$$

Motor torque T_e can be generated by the current i_q, as in (5).

1) Currents Bias: In practice, when two of the three-phase stator currents i_a and i_b are with biases ΔB and ΔC, respectively, the third current i_c is calculated directly from its balance relationship as

$$\begin{cases} i_a = A\sin\omega_e t + \Delta B \\ i_b = A\sin(\omega_e t + 2\pi/3) + \Delta C \\ i_c = A\sin(\omega_e t - 2\pi/3) - \Delta B - \Delta C \end{cases} \tag{18}$$

where $\omega_e = (P/2)\omega$, and P is the pole number of the motor. Thus

$$\begin{cases} i_d = 0 + \sqrt{\Delta B^2 + \Delta D^2}\sin(\omega_e t + \varphi) \\ i_q = A + \sqrt{\Delta B^2 + \Delta D^2}\cos(\omega_e t + \varphi) \end{cases} \tag{19}$$

where $\Delta D = (\Delta B + 2\Delta C)/\sqrt{3}$, and $\varphi = \tan^{-1}(\Delta B/\Delta D)$. Therefore, components at the rotational frequency will present and cause torque ripple.

2) Mismatched Amplitude: When the measured currents present different gains or amplitudes for the measured currents i_a and i_b as

$$\begin{cases} i_a = \widetilde{A}\sin\omega_e t \\ i_b = \widetilde{B}\sin(\omega_e t + 2\pi/3) \\ i_c = -\widetilde{A}\sin\omega_e t - \widetilde{B}\sin(\omega_e t + 2\pi/3) \end{cases} \tag{20}$$

where $\widetilde{A}$ and $\widetilde{B}$ are the nonunit amplitudes corresponding to phases A and B, respectively. By substituting (20) into the

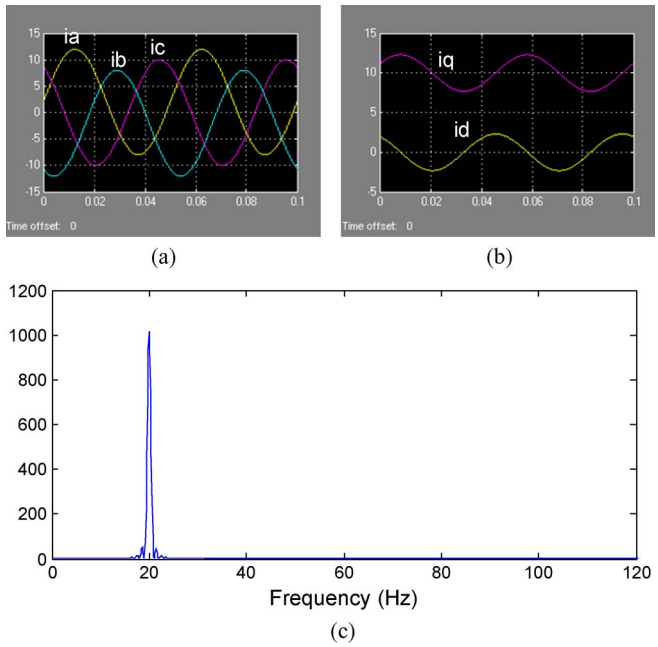

Fig. 6. Simulation as the three-phase currents with bias. (a) abc current. (b) dq current. (c) FFT from dq current.

Clarke and Park transform, the two-phase currents i_d and i_q are obtained as

$$\begin{cases} i_d = -\widetilde{E} + \sqrt{\widetilde{D}^2 + \widetilde{E}^2}\sin(2\omega_e t + \varphi) \\ i_q = -\frac{\widetilde{A}}{2} + \frac{\widetilde{B}}{2} + \sqrt{\widetilde{D}^2 + \widetilde{E}^2}\cos(2\omega_e t + \varphi) \end{cases} \tag{21}$$

where

$$\widetilde{D} = (\widetilde{A} + \widetilde{B})/2$$
$$\widetilde{E} = -\widetilde{C}/2$$
$$\phi = \tan^{-1}(\widetilde{E}/\widetilde{D}).$$

Thus, the component corresponding to the rotational speed will also contribute to the torque ripple with the component $2\omega_e$. Therefore, with both bias and mismatched amplitude of the current measurements, two components of ω_e and $2\omega_e$ will manifest in a constant speed operation.

B. Simulation Results

The bias and mismatched amplitudes among the measured currents will also present components related to its rotational frequency. For example, if the rotational speed is 5 r/s (300 rpm) with the eight-pole motor, the i_d and i_q will produce the frequency of $4(\text{pole pair}) \times 5(\text{r/s}) = 20$ Hz for the case where bias exists, as shown in Fig. 6. As both bias and mismatched amplitudes occur, $4(\text{pole pair}) \times 2 \times 5(\text{r/s}) = 40$ Hz, as well as the 20 Hz, will be observed together, as shown in Fig. 7. These simulation results are in agreement with the analytical results that can be achieved through (19) and (21).

C. Suppression of Torque Ripple

As discussed earlier, given that bias and mismatch gains for three current measurements exist, the effect of the torque ripple will manifest as the motor rotates at a certain speed. Therefore, the notch filter with a fixed frequency band is not suitable for

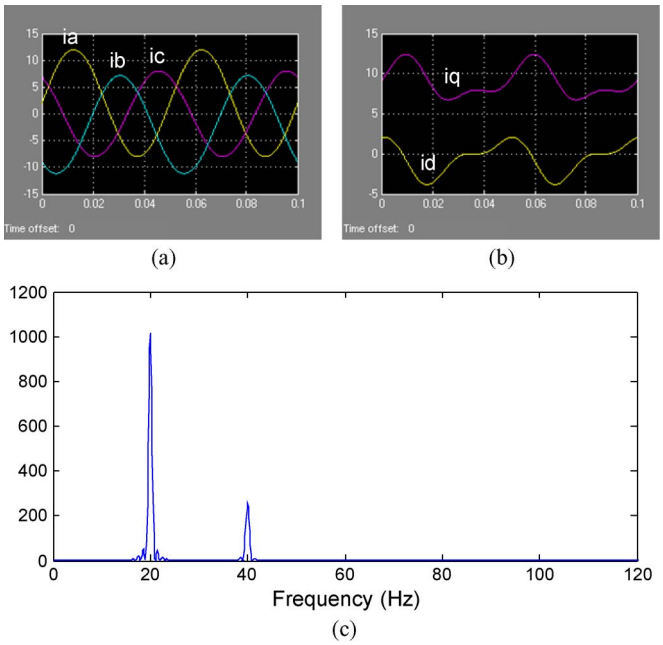

Fig. 7. Simulation as the three-phase currents with mismatched amplitudes. (a) abc current. (b) dq current. (c) FFT from dq current.

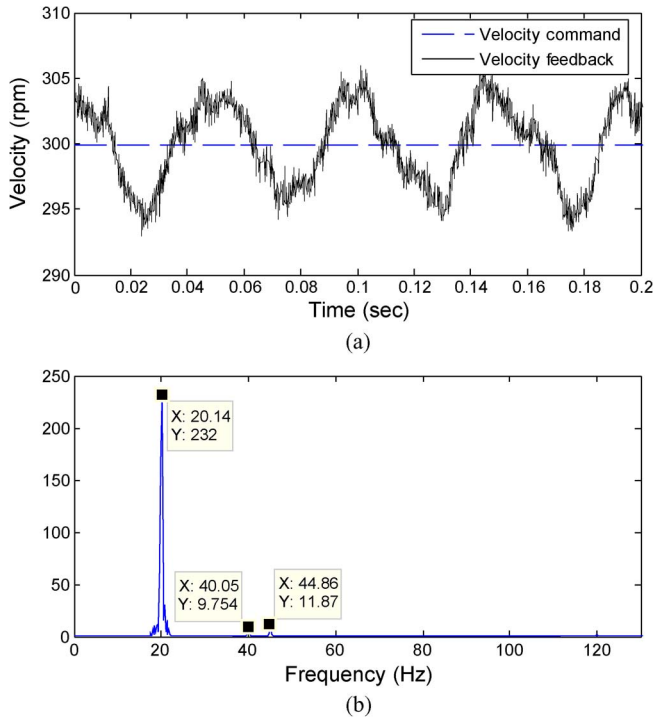

Fig. 8. Results of the servomotor operating at 300 r/min. (a) Steady-state response. (b) FFT.

eliminating the torque ripple effect of servomotors generally operated with varied speeds. In this paper, the state-space DOB in addition to the original PI controller has been implemented to suppress the ripples without the knowledge of the motor operation commands. Experimental results for the present servomotor with 300 r/min are shown in Fig. 8. Its fast Fourier transform (FFT) indicates that two peaks with frequencies at 20 and 40 Hz can be observed. The present experimental results are in good agreement with the previously achieved simulation and analytical results. By implementing the DOB

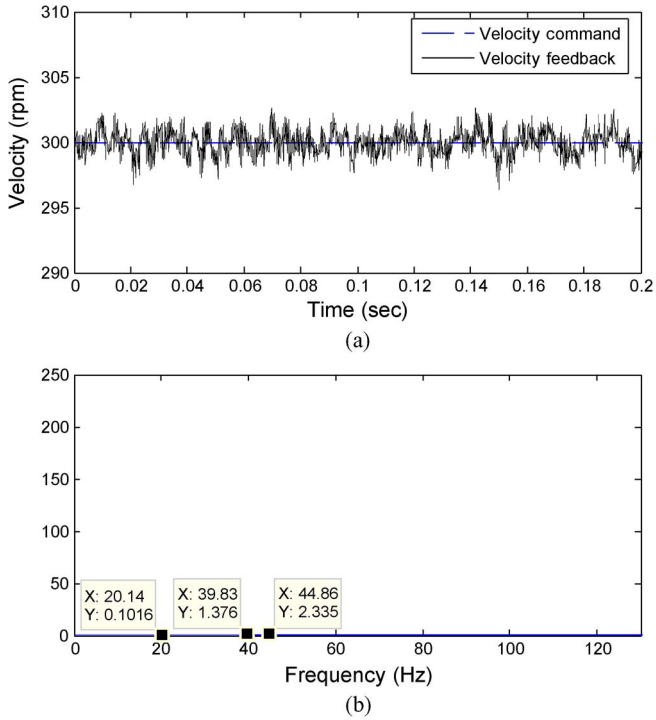

Fig. 9. Results of the servomotor applying the DOB. (a) Steady-state response. (b) FFT.

Fig. 10. DYNA DM1007 CNC machine tool.

with relatively fast poles at 1000 rad/s, the present DOB-based design shows desirable velocity responses by suppressing undesirable components, as shown in Fig. 9.

IV. Precision Motion on CNC

The developed DOB-based servomotor control on the Tamagawa 400-W servomotor and the 17-bit encoder were further implemented on a DYNA DM1007 CNC machine tool, as shown in Fig. 10. Experimental results indicate that, in addition to controlling the servomotors, the motion friction between the machine table and the guide is also achieved, which resulted in degrading the contouring precision seriously.

A. Online Estimation of Friction

The friction effect becomes more significant as the servomotor is implemented on the CNC machine table and manifests

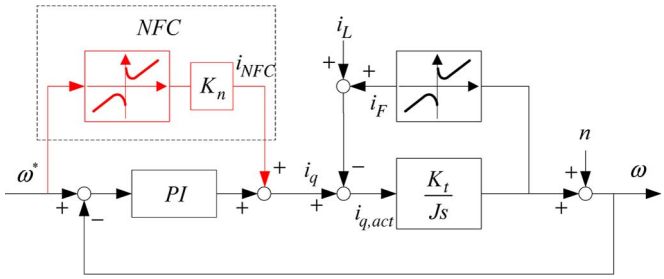

Fig. 11. Block diagram of the NFC for friction.

as either a slip-stick effect with a circular motion or quadrant glitches [19], [20]. Although the applications of the DOB suppress the friction effect based on the linear modeling [17], the friction compensation should be further adopted with a nonlinear structure. In recent literature on model-based nonlinear compensation, nonlinear models with more extensive structures, as well as a number of parameters to be identified, have already been proposed [18], [21]–[23]. In practice, to avoid the high integral gain as the speed approaches zero with significant nonlinear friction [24], the proposed NFC is not activated in order to compensate for the friction effect as the speed within ± 1 r/min. Thus, smoother contouring performance can be achieved empirically. The friction model with a higher bandwidth requires more accurate parameter identification process; however, it may be sensitive to parameter variations [25]. In this paper, the velocity loop of servomotors is shown in Fig. 11, and an effective NFC structure is likewise shown in the figure. Theoretically, the generated torque by the motor is intended to reduce the effects of the friction and the external disturbance when they become serious; the measured motor current $i_{q,\mathrm{act}}$ is expressed as

$$i_{q,\mathrm{act}} = i_q - i_F - i_L \tag{22}$$

where i_L is the external disturbance, and i_F is the sum of static, Coulomb, and viscous friction. Without considering the cutting force, i_L is considered negligible, and the mechanical equation is expressed as

$$J\frac{d\omega}{dt} = K_t i_{q,\mathrm{act}} = K_t(i_q - i_F). \tag{23}$$

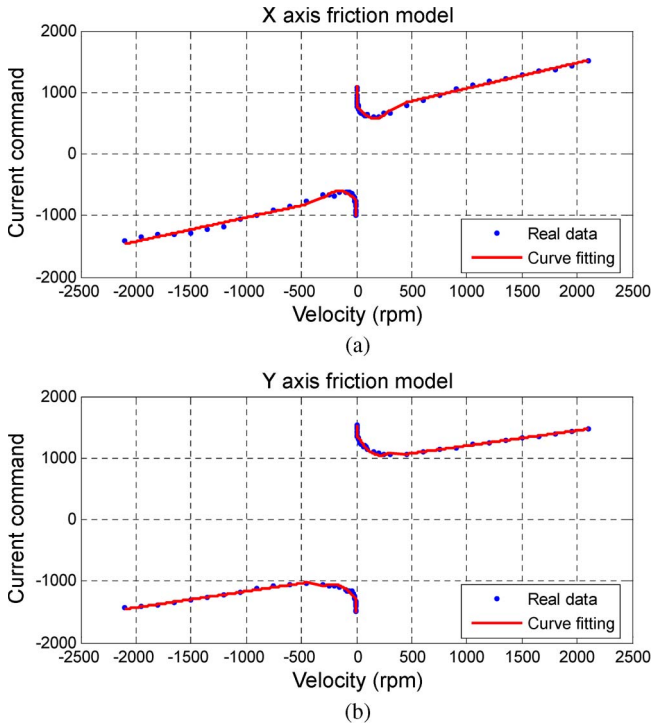

Fig. 12. Estimated friction for (a) X and (b) Y axes.

Under constant speed testing, the measured i_q is equal to the equivalent friction of i_F. Moreover, by applying different velocity commands to the servo driver, the nonlinear friction curve with different speeds can be achieved by measuring the corresponding current commands when the motor speed reaches its steady state. Then, the feedforward NFC is obtained to compensate for the friction effect by providing an extra current command, as shown in Fig. 11.

Experimental results that help identify friction for the X and Y axes separately are shown in Fig. 12. The friction models for the X and Y axes can be obtained separately by applying the least square curve fitting, as detailed in the following:

1) X axis, given by (24), shown at the bottom of the page;
2) Y axis, given by (25), shown at the bottom of the page.

$$i_{x,\mathrm{NFC}} = \begin{cases} \bullet(1)\ -5.07669\omega + 1131.70743, & 1 \le \omega < 5 \text{ r/min} \\ \bullet(2)\ 0.000065155\omega^2 - 0.2444\omega + 806.7031, & 5 < \omega < 450 \text{ r/min} \\ \bullet(3)\ 0.037967\omega + 648.48695, & 450 \le \omega < 3000 \text{ r/min} \\ \bullet(4)\ -2.77035\omega - 1020.48697, & -1 \ge \omega > -5 \text{ r/min} \\ \bullet(5)\ -0.000051436\omega^2 - 0.18661\omega - 770.91, & -5 > \omega > -450 \text{ r/min} \\ \bullet(6)\ 0.03569\omega - 638.52035, & -450 \ge \omega > -3000 \text{ r/min} \end{cases} \tag{24}$$

$$i_{y,\mathrm{NFC}} = \begin{cases} \bullet(1)\ -1.45379\omega + 1536.73997, & 1 \le \omega < 5 \text{ r/min} \\ \bullet(2)\ 0.000056286\omega^2 - 0.27681\omega + 1382.7587, & 5 < \omega < 450 \text{ r/min} \\ \bullet(3)\ 0.022665\omega + 949.65453, & 450 \le \omega < 3000 \text{ r/min} \\ \bullet(4)\ -2.48836\omega - 1513.58364, & -1 \ge \omega > -5 \text{ r/min} \\ \bullet(5)\ -0.0000432\omega^2 - 0.21424\omega - 1315.8638, & -5 > \omega > -450 \text{ r/min} \\ \bullet(6)\ 0.023978\omega - 902.19512, & -450 \ge \omega > -3000 \text{ r/min} \end{cases} \tag{25}$$

B. Contouring With Integrated Control

Contouring accuracy by integrating different motion controllers was verified with the circular command in 10-mm radius at 1200 and 2400 mm/min, respectively. Furthermore, the XY table with a 16-kg load was also tested to verify the present control under external loading conditions. Experimental results, as shown in Fig. 13, indicate that the motion precision of the basic PI control in the original CNC machine tool was greatly improved by integrating DOB and NFC, as shown in Fig. 13(b) and (c). Results show that the PI controller added with the DOB resulted in significantly improved oscillation of the circular trajectory, as shown in Fig. 13(b). Thus, the repeatability of motion performance can be improved, so that the prediction of the friction effect can be more suitably obtained. When the NFC was further added, its contouring errors caused by the slip-stick effect were greatly improved, as shown in Fig. 13(c).

With a negligible viscous coefficient, the velocity open loop with a PI controller can be expressed as

$$K_{\nu p}\left(1+\frac{K_{\nu i}}{s}\right)\cdot\frac{1}{\hat{J}s}=\frac{K_{\nu p}}{\hat{J}}\left(\frac{s+K_{\nu i}}{s}\right). \tag{26}$$

Thus, a suitable control gain of the velocity loop can be directly determined by increasing the gain of the estimated inertia. Therefore, when the system integrated all autotuned $PI+DOB+NFC$ with a doubled gain, experimental results indicate that the roundness error of circular trajectory was reliably reduced from 13.3 to 2.0 μm, as shown in Fig. 13(d). Results are also summarized in Fig. 14 to indicate the superiority and feasibility of the present design for CNC machine tools.

C. Speed and Loading Effects

In general, the motion accuracy of CNC machine tools increases as the operating speed increases. Compared with traditional PI controllers, the experimental results shown in Fig. 15(a) indicate that the robustness of the proposed controller is improved under different speeds. Moreover, an extra load was added to verify the robustness of the present control implementation against the external load of 16 kg, as shown in Fig. 15(b). In general, the higher feed rate and the extra loading will lead to larger motion error for PI controllers. With the proposed integrated design, results show that the motion accuracy with the DOB and NFC is robust against both varied loading and speed.

D. Discussions

Empirical results indicate that, without considering the geometric error of the machine table, the contouring error estimation caused from the servo tracking error is about the same order with that measured directly from the double ball bar. For the system without the DOB application, although the implementation of NFC also decreased the slip-stick effect, as shown

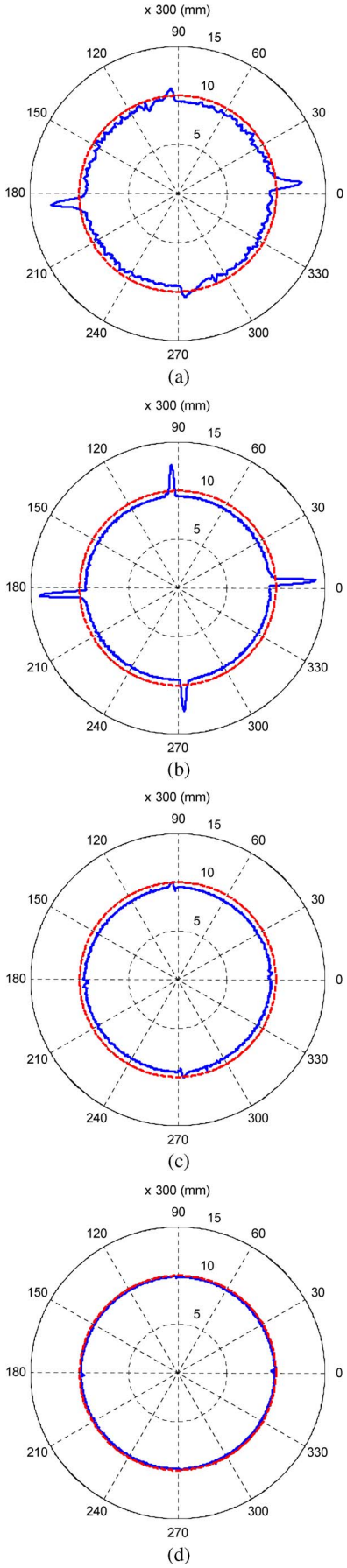

Fig. 13. Contouring accuracy with different controllers. (a) PI controller. (b) $PI+DOB$. (c) $PI+DOB+NFC$. (d) Tuned $PI+DOB+NFC$.

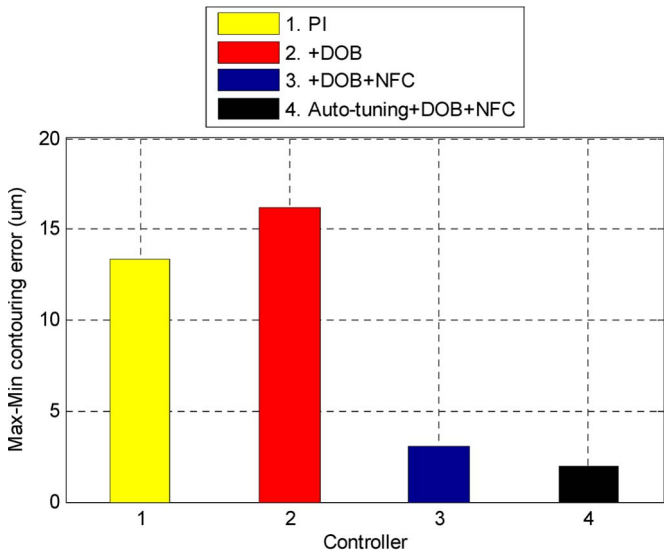

Fig. 14. Roundness error with different controllers.

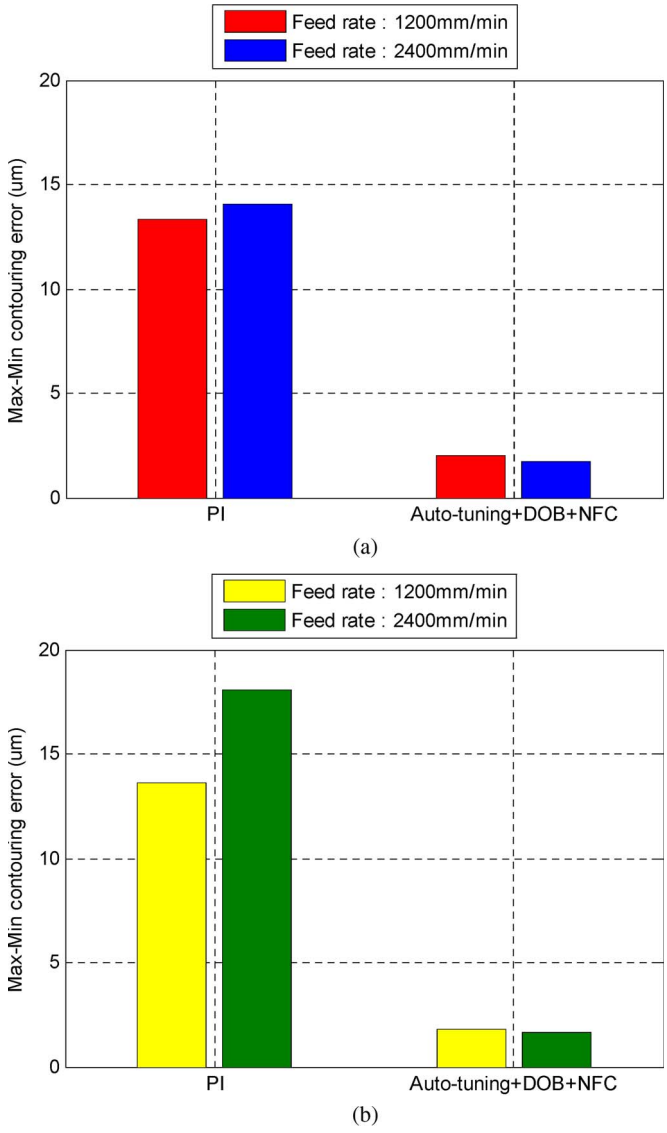

Fig. 15. Roundness error for different feed rates. (a) Without load. (b) With a 16-kg load.

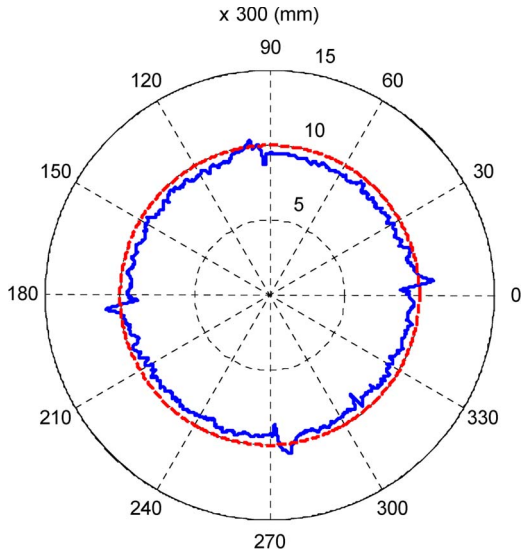

Fig. 16. Contouring results of $PI + NFC$ without DOB.

in Fig. 16, the compensated system became more unstable, and its precision is not significantly improved. However, as shown in Fig. 13(b), the DOB successfully suppressed the contouring oscillation, and the system became more stable and repeatable. Therefore, the motion for the system that applies DOB is in a more linear nature, and the corresponding uncertainties can thus be reduced. Therefore, the additional implementation of the nonlinear NFC became more effective to improve the slip-stick motion error, as shown in Fig. 13(c). Moreover, the proportional gain in the outset positional loop can be directly increased to achieve great improvement in contouring precision.

V. Conclusion

In this paper, the uncertainty effects of parameter variation, measurement error, and external disturbance of servomotors on both the current and velocity loops have been studied for the servomotor with significantly improved suppression of the torque ripple effect by applying the DOB. Furthermore, the variation owing to the inertia and viscous friction coefficient can also be observed through the output of DOB. An autotuning process has also been developed accordingly.

In addition to the linear estimation and compensation approach of DOB for the inner current and velocity loops, a practical nonlinear NCF integrated with the DOB has been successfully proposed for a CNC machine tool to effectively suppress the slip-stick effect on the circular contouring due to friction. Results show that the contouring precision of the machine tool has been significantly improved, and its roundness error has been greatly reduced from 13.3 to 2.0 μm. Extensive experimental results on the CNC machine tool also indicate that, by applying the present control, the roundness of contouring precision can be maintained well even at a higher speed under loading condition. This proves the feasibility of the proposed control and compensation design in real applications.

REFERENCES

[1] D. W. Novotny and T. A. Lipo, *Vector Control and Dynamics of AC Drives*. Oxford, U.K.: Clarendon, 1996.

[2] B. K. Bose, *Modern Power Electronics and AC Drives*. Englewood Cliffs, NJ: Prentice-Hall, 2002.

[3] Y. Koren, "Cross-coupled biaxial computer for manufacturing systems," *Trans. ASME, J. Dyn. Syst., Meas. Control*, vol. 102, no. 4, pp. 265–272, Dec. 1980.

[4] M. Tomizuka, "Zero phase error tracking algorithm for digital control," *Trans. ASME, J. Dyn. Syst., Meas. Control*, vol. 109, no. 1, pp. 65–68, Mar. 1987.

[5] S. S. Yeh and P. L. Hsu, "Theory and applications of the robust cross-coupled control design," *Trans. ASME, J. Dyn. Syst., Meas. Control*, vol. 121, no. 3, pp. 524–530, Sep. 1999.

[6] S. S. Yeh and P. L. Hsu, "Estimation of the contouring error vector for the cross-coupled control design," *IEEE/ASME Trans. Mechatronics*, vol. 7, no. 1, pp. 44–51, Mar. 2002.

[7] G. F. Franklin, J. D. Powell, and M. Workman, *Digital Control of Dynamic Systems*, 3rd ed. Reading, MA: Addison-Wesley, 1998.

[8] H. Kobayashi, S. Katsura, and K. Ohnishi, "An analysis of parameter variations of disturbance observer for motion control," *IEEE Trans. Ind. Electron.*, vol. 54, no. 6, pp. 3413–3421, Dec. 2007.

[9] S. Katsura, K. Irie, and K. Ohishi, "Wideband force control by position-acceleration integrated disturbance observer," *IEEE Trans. Ind. Electron.*, vol. 55, no. 4, pp. 1699–1706, Apr. 2008.

[10] K. B. Lee and F. Blaabjerg, "Robust and stable disturbance observer of servo system for low-speed operation," *IEEE Trans. Ind. Appl.*, vol. 43, no. 3, pp. 627–635, May/Jun. 2007.

[11] J. H. She, M. Fang, Y. Ohyama, H. Hashimoto, and M. Wu, "Improving disturbance-rejection performance based on an equivalent-input-disturbance approach," *IEEE Trans. Ind. Electron.*, vol. 55, no. 1, pp. 380–389, Jan. 2008.

[12] K. J. Yang, Y. J. Choi, and W. K. Chung, "On the tracking performance improvement of optical disk drive servo systems using error-based disturbance observer," *IEEE Trans. Ind. Electron.*, vol. 52, no. 1, pp. 270–279, Feb. 2005.

[13] K. Ohishi, T. Miyazaki, K. Inomata, H. Yanagisawa, D. Koide, and H. Tokumaru, "Robust tracking servo system considering force disturbance for the optical disk recording system," *IEEE Trans. Ind. Electron.*, vol. 53, no. 3, pp. 838–847, Jun. 2006.

[14] T. M. O'Sullivan, C. M. Bingham, and N. Schofield, "Observer-based tuning of two-inertia servo-drive systems with integrated SAW torque transducers," *IEEE Trans. Ind. Electron.*, vol. 54, no. 2, pp. 1080–1091, Apr. 2007.

[15] A. Kamalzadeh and K. Erkorkmaz, "Accurate tracking controller design for high-speed drives," *Int. J. Mach. Tools Manuf.*, vol. 47, no. 9, pp. 1393–1400, Jul. 2007.

[16] R. Cardenas, R. Pena, G. M. Asher, J. Clare, and R. Blasco-Gimenez, "Control strategies for power smoothing using a flywheel driven by a sensorless vector-controlled induction machine operating in a wide speed range," *IEEE Trans. Ind. Electron.*, vol. 51, no. 3, pp. 603–614, Jun. 2004.

[17] S. M. Yang and Y. J. Deng, "Observer-based inertial identification for auto-tuning servo motor drives," in *Conf. Rec. 40th IEEE IAS Annu. Meeting*, Oct. 2–6, 2005, vol. 2, pp. 968–972.

[18] A. H. Brian, D. Pierre, and C. de W. Carlos, "A survey of models, analysis tools and compensation methods for the control of machines with friction," *Automatica*, vol. 30, no. 7, pp. 1083–1138, Jul. 1994.

[19] Z. Jamaludin, H. Van Brussel, and J. Swevers, "Quadrant glitch compensation using friction model-based feedforward and an inverse-model-based disturbance observer," in *Proc. 10th IEEE Adv. Motion Control*, Trento, Italy, Mar. 26–28, 2008, pp. 212–217.

[20] S. S. Yeh and P. L. Hsu, "Perfectly matched feedback control and its integrated design for multiaxis motion systems," *Trans. ASME, J. Dyn. Syst. Meas. Control*, vol. 126, no. 3, pp. 547–557, Sep. 2004.

[21] C. T. Johnson and R. D. Lorenz, "Experimental identification of friction and its compensation in precise, position controlled mechanisms," *IEEE Trans. Ind. Appl.*, vol. 28, no. 6, pp. 1392–1398, Nov./Dec. 1992.

[22] L. Márton and B. Lantos, "Modeling, identification, and compensation of stick-slip friction," *IEEE Trans. Ind. Electron.*, vol. 54, no. 1, pp. 511–521, Feb. 2007.

[23] D. D. Rizos and S. D. Fassois, "Friction identification based upon the LuGre and Maxwell slip models," *IEEE Trans. Control Syst. Technol.*, vol. 17, no. 1, pp. 150–160, Jan. 2009.

[24] D. H. Lee and J. W. Ahn, "Dual speed control scheme of servo drive system for a nonlinear friction compensation," *IEEE Trans. Power Electron.*, vol. 23, no. 2, pp. 959–965, Mar. 2008.

[25] A. Ramasubramanian and L. R. Ray, "Comparison of EKBF-based and classical friction compensation," *Trans. ASME, J. Dyn. Syst., Meas. Control*, vol. 129, no. 2, pp. 236–242, Mar. 2007.

Wei-Sheng Huang received the B.S. degree in nuclear engineering from National Tsing Hua University, Hsinchu, Taiwan, in 1986, and the M.S. degree in information engineering from National Chiao Tung University, Hsinchu, in 1993, where he is currently working toward the Ph.D. degree in the Institute of Electrical and Control Engineering.

In 1988, he was with the Mechanical Industry Research Laboratory, Industrial Technology Research Institute, Hsinchu. During this time, he was engaged in research and development work on optical players and numerical controllers of machine tools. He is currently a Principal Engineer with the Numerical Controller Research Division, Syntec, Hsinchu, where he is engaged in system software development of numerical controllers. His research with specialization in high-speed–high-precision motion control includes motion control, industrial networks, optomechatronics, machine vision and robots.

Chun-Wei Liu received the B.S. degree in electrical engineering from National Yunlin University of Science and Technology, Douliu, Taiwan, in 2006, and the M.S. degree from the Institute of Electrical and Control Engineering, National Chiao Tung University, Hsinchu, Taiwan, in 2008.

He is currently serving in the military of the Republic of China. His research interests include motion control, autotuning, and remote diagnosis.

Pau-Lo Hsu (M'91) received the B.S. degree in mechanical engineering from National Cheng Kung University, Tainan, Taiwan, in 1978, the M.S. degree in mechanical engineering from the University of Delaware, Newark, in 1984, and the Ph.D. degree in mechanical engineering from the University of Wisconsin, Madison, in 1987.

Following two years of military service in King-Men, he was with San-Yang (Honda) Industry during 1980–1981 and Sandvik (Taiwan) during 1981–1982. In 1988, he joined the Department of Electrical and Control Engineering, National Chiao Tung University, Hsinchu, Taiwan, as an Associate Professor, where he was the Chairman during 1998–2000 and has been a Professor since 1995. His research interests include computerized numerical control motion control, servo systems, diagnostic systems, and network control systems.

Syh-Shiuh Yeh received the B.S. degree in mechanical engineering and the M.S. and Ph.D. degrees in electrical and control engineering from National Chiao Tung University, Hsinchu, Taiwan, in 1994, 1996, and 2000, respectively.

He was a Researcher with the Mechanical Industry Research Laboratory, Industrial Technology Research Institute, Hsinchu. He is currently an Assistant Professor in the Department of Mechanical Engineering, National Taipei University of Technology, Taipei, Taiwan. His research interests include control design of multiaxis motion systems, design and control of mobile robots, actuator and sensor design for robot applications, and human–robot interaction.